Integrated metabolic spatial-temporal model for the prediction of ammonia detoxification during liver damage and regeneration

Freimut Schliess, Stefan Hoehme, Sebastian Henkel, Ahmed Ghallab, Dominik Driesch, Jan Böttger, Reinhard Guthke, Michael Pfaff, Jan Hengstler, Rolf Gebhardt, et al.

HEPATOLOGY
Official Journal of the American Association for the Study of Liver Diseases

Integrated Metabolic Spatial-Temporal Model for the Prediction of Ammonia Detoxification During Liver Damage and Regeneration

Freimut Schliess,[1]* Stefan Hoehme,[2]* Sebastian G. Henkel,[4]* Ahmed Ghallab,[5]* Dominik Driesch,[4] Jan Böttger,[3] Reinhard Guthke,[6] Michael Pfaff,[4] Jan G. Hengstler,[5] Rolf Gebhardt,[3] Dieter Häussinger,[1] Dirk Drasdo,[2,7,8] and Sebastian Zellmer[3]

The impairment of hepatic metabolism due to liver injury has high systemic relevance. However, it is difficult to calculate the impairment of metabolic capacity from a specific pattern of liver damage with conventional techniques. We established an integrated metabolic spatial-temporal model (IM) using hepatic ammonia detoxification as a paradigm. First, a metabolic model (MM) based on mass balancing and mouse liver perfusion data was established to describe ammonia detoxification and its zonation. Next, the MM was combined with a spatial-temporal model simulating liver tissue damage and regeneration after CCl_4 intoxication. The resulting IM simulated and visualized whether, where, and to what extent liver damage compromised ammonia detoxification. It allowed us to enter the extent and spatial patterns of liver damage and then calculate the outflow concentrations of ammonia, glutamine, and urea in the hepatic vein. The model was validated through comparisons with (1) published data for isolated, perfused livers with and without CCl_4 intoxication and (2) a set of *in vivo* experiments. Using the experimentally determined portal concentrations of ammonia, the model adequately predicted metabolite concentrations over time in the hepatic vein during toxin-induced liver damage and regeneration in rodents. Further simulations, especially in combination with a simplified model of blood circulation with three ammonia-detoxifying compartments, indicated a yet unidentified process of ammonia consumption during liver regeneration and revealed unexpected concomitant changes in amino acid metabolism in the liver and at extrahepatic sites. *Conclusion:* The IM of hepatic ammonia detoxification considerably improves our understanding of the metabolic impact of liver disease and highlights the importance of integrated modeling approaches on the way toward virtual organisms. (HEPATOLOGY 2014;60:2040-2051)

Abbreviations: Arg, arginine; Asp, aspartate; $C_A(t)$, concentration at position A; $C_{AB}(t)$, concentration at a given point in space between A and B; $C_{AC}(t)$, concentration at a given point in space between A and C; $C_B(t)$, concentration at position B; $C_{BC}(t)$, concentration at a given point in space between B and C; $C_C(t)$, concentration at position C; $c_{j,k}$, measured output concentrations for $j = \{$glutamine, NH4, urea$\}$ and $k = 1, \ldots, 13$ experiments; $\hat{c}_{j,k}$, simulated parameter-dependent output concentrations for $j = \{$glutamine, NH_4, urea$\}$ and $k = 1, \ldots, 13$ experiments; c_{Gln}, concentration of glutamine; $c_{Gln,in}$, inflow concentration of glutamine; $c_{Gln,out}$, outflow concentration of glutamine; $c_{Gln,pc}$, concentration of glutamine in the pericentral compartment; $c_{Gln,pp}$, concentration of glutamine in the periportal compartment; c_{NH4}, concentration of NH_4^+; $c_{NH4,in}$, inflow concentration of NH_4^+; $c_{NH4,out}$, outflow concentration of NH_4^+; $c_{NH4,pc}$, concentration of NH_4^+ in the pericentral compartment; $c_{NH4,pp}$, concentration of NH_4^+ in the periportal compartment; CPS, carbamoyl phosphate synthetase; c_{Urea}, concentration of urea; $c_{Urea,in}$, inflow concentration of urea; $c_{Urea,out}$, outflow concentration of urea; $c_{Urea,pc}$, concentration of urea in the pericentral compartment; $c_{Urea,pp}$, concentration of urea in the periportal compartment; F, transported volume per unit of time; F_{mL}, perfusion volume flow rate per liver mass; Gln, glutamine; GLNase, glutaminase; Glu, glutamate; GS, glutamine synthetase; h, approximate average height of a lobule; IM, integrated metabolic spatial-temporal model; $K_{AG,Gln}$, dissociation constant of glutaminase glutamine; $K_{i,GS,Gln}$, inhibition constant of GS glutamine; $K_{m,C,NH4}$, Michaelis constant of carbamoyl phosphate synthetase ammonia; $K_{m,G,NH4}$, Michaelis constant of glutaminase ammonia; $K_{m,GS,NH4}$, Michaelis constant of glutamine synthetase ammonia; L, average hepatocyte diameter; MM, metabolic model; n, Hill coefficient; N, number of hepatocytes per unit of area within a liver lobule; N_{pc}, pericentral number of hepatocytes in a cross-section of a liver lobule; N_{pp}, periportal number of hepatocytes in a cross-section of a liver lobule; q, least squares; SD, standard deviation; STM, spatial-temporal model; $t_{i,i+1}$, given point in time between t_i and t_{i+1}; v_C, synthesis rate of urea; v_G, glutaminase-catalyzed glutamine degradation rate; v_{GS}, glutamine synthesis rate; v_H, hepatocyte volume; $v_{max,C}$, maximal synthesis rate of urea; $v_{max,G}$, maximal rate of glutamine degradation; $v_{max,GS}$, maximal rate of glutamine synthesis; $v_{NH4,endo}$, production rate of released endogenous ammonia; V_{pc}, volume of the pericentral region; V_{pp}, volume of the periportal region; V_x, volume of compartment x; x_A, minimal distance of that point to A; x_B, minimal distance of a point to B; x_C, minimal distance of a point to C.

See Editorial on Page 1823

The impairment of hepatic ammonia detoxification in the diseased liver is a key event in the pathogenesis of hepatic encephalopathy.[1] Hepatic ammonia consumption by the synthesis of both urea and glutamine (Gln) is critical for keeping systemic ammonia levels low. In the intact liver lobule, urea synthesis and Gln synthesis are anatomically arranged in series[2-8] (Fig. 1A). Through the use of bidirectional (antegrade and retrograde) rat liver perfusion, the concept of intercellular Gln cycling [i.e., the glutaminase (GLNase)-catalyzed deamidation of Gln in periportal hepatocytes and the glutamine synthetase (GS)–catalyzed resynthesis of Gln in pericentral scavenger cells] has been established.[2,9] Under normal conditions, periportal Gln breakdown and pericentral Gln synthesis are well balanced. Under pathological conditions such as sepsis, liver cirrhosis, and CCl_4 or acetaminophen intoxication, a scavenger cell defect essentially contributes to the development of hyperammonemia,[1,4-6,10] which is potentially life-threatening.[11]

Modeling of hepatic urea metabolism started more than 30 years ago,[12] but it remained limited because acinar compartmentation had not yet been elucidated. Later, acinar compartmentalization of ammonia metabolism was integrated into the modeling of the hepatic contribution to systemic acid-base homeostasis.[13] Recently, spatial-temporal models (STMs) of liver tissue have been developed.[14-16] These models consider hepatocytes and sinusoids of a liver lobule as well as the principles of how individual cells interact in order to establish functional tissue microarchitecture. They can be used to simulate, for example, the destruction and regeneration process of a liver lobule after the administration of CCl_4, but they lack the ability to simulate spatial-temporal profiles of metabolites.

To bridge this gap, a two-compartment metabolic model (MM) of ammonia, urea, and Gln metabolism was developed (Fig. 1B), and it was integrated into an STM of liver regeneration.[15] Moreover, the published version of the STM, comprising only a single liver lobule, was extended to a group of seven lobules. To achieve this goal, the following strategy was applied (Fig. 2):

1. Mouse liver perfusion experiments were performed with different concentrations of ammonia and Gln in antegrade and retrograde directions of both intact and impaired tissue, and the effluent concentrations of ammonia, Gln, and urea were thereby monitored. The resulting perfusion data, complemented by available biological knowledge (e.g., the stoichiometry of metabolic reactions), were used to establish an MM of ammonia detoxification in the intact murine liver.
2. The recently established STM for liver regeneration after CCl_4-induced damage in mice[15] was applied to simulate the volumes of GS-active, GS-inactive,

From the [1]Clinic for Gastroenterology, Hepatology, and Infectiology, Heinrich Heine University, Düsseldorf, Germany; [2]Interdisciplinary Center for Bioinformatics, University of Leipzig, Leipzig, Germany; [3]Institute of Biochemistry, Faculty of Medicine, University of Leipzig, Leipzig, Germany; [4]BioControl Jena GmbH, Jena, Germany; [5]Leibniz Research Centre for Working Environment and Human Factors, Dortmund, Germany; [6]Leibniz Institute for Natural Product Research and Infection Biology Hans Knoell Institute, Jena, Germany; [7]INRIA, Le Chesnay, France; [8]Jacques-Luis Lions Laboratory, National Center of Scientific Research Joint Research Unit 7598, Pierre and Marie Curie University, Paris, France.

Received August 21, 2013; accepted March 14, 2014.

Additional Supporting Information may be found at onlinelibrary.wiley.com/doi/10.1002/hep.27136/suppinfo.

This work was cofunded by the Virtual Liver Initiative (www.virtual-liver.de) of the German Federal Ministry of Education and Research, Collaborative Research Center 974 (Communication and Systems Relevance of Liver Damage and Regeneration), and the European Union Seventh Framework Programme for Research (projects NOTOX [Predicting long-term toxic effects using computer models based on systems characterization of organotypic cultures, http://notox-sb.eu/welcome/] and PASSPORT [PAtient Specific Simulation and PreOperative Realistic Training for liver surgery, http://www.passport-liver.eu/Homepage.html]).

**These authors contributed equally to this work.*

Dirk Drasdo and Sebastian Zellmer share senior authorship.

Freimut Schliess is currently affiliated with Profil Institute for Metabolic Research GmbH, Neuss, Germany.

Ahmed Ghallab's secondary address is the Faculty of Veterinary, Medicine, South Valley University, Qena, Egypt.

Michael Pfaff is currently affiliated with the Department of Medical Engineering and Biotechnology, University of Applied Sciences Jena, Jena, Germany.

Sebastian Zellmer is currently affiliated with the Department of Product Safety, German Federal Institute for Risk Assessment, Berlin, Germany.

Address reprint requests to: Dirk Drasdo, Ph.D., INRIA, BP 105, 8153 Le Chesnay Cedex, France. E-mail: dirk.drasdo@inria.fr; or Sebastian Zellmer, Ph.D., Department of Product Safety, German Federal Institute for Risk Assessment, Max-Dohrn Strasse 8-10, 10589 Berlin, Germany. E-mail: sebastian.zellmer@bfr.bund.de.

View this article online at wileyonlinelibrary.com.

DOI 10.1002/hep.27136

Potential conflict of interest: Dr. Pfaff owns stock in BioControl Jena.

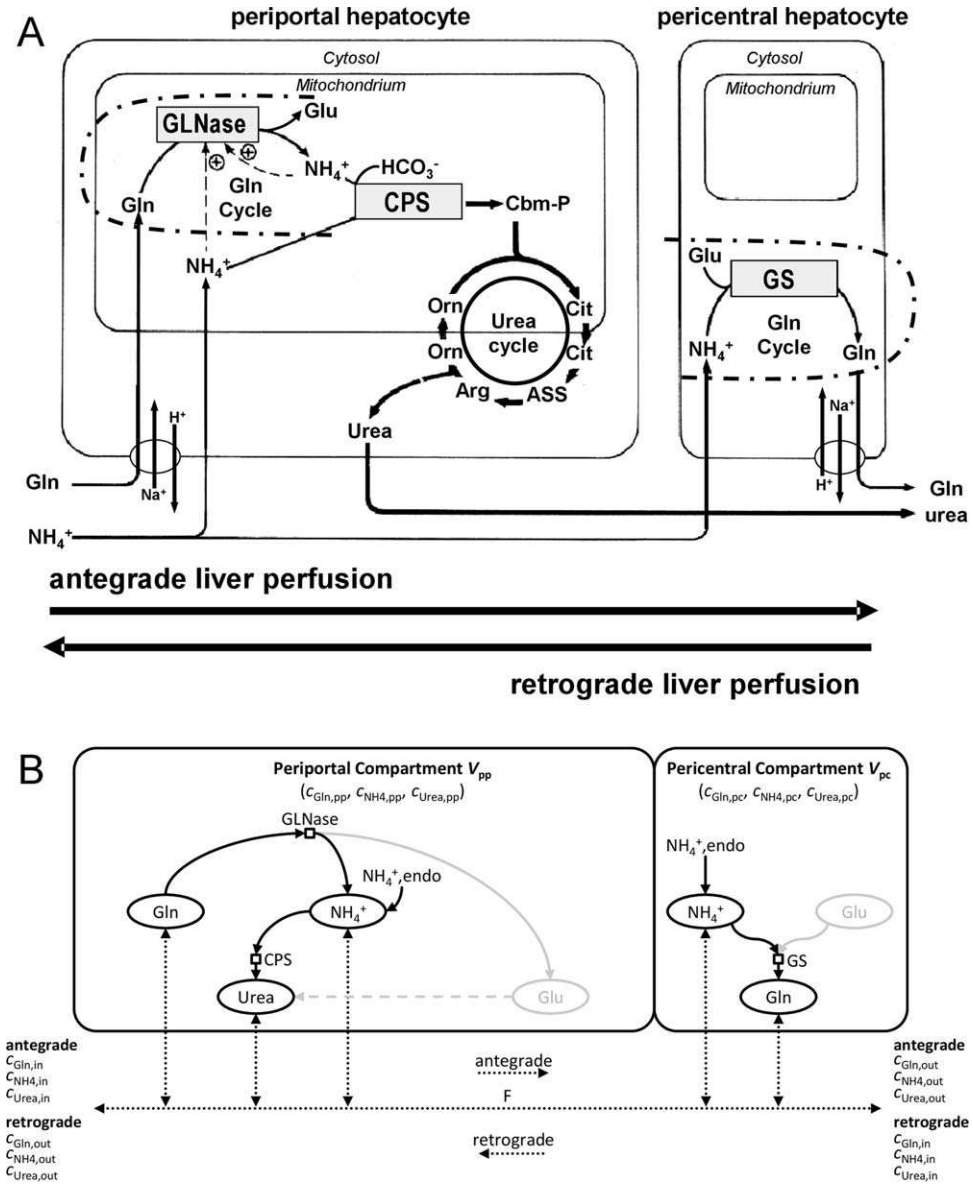

Fig. 1. Acinar compartmentation of ammonia detoxification in the intact liver. (A) Gln cycling. Periportal GLNase and pericentral GS are simultaneously active, and this results in periportal breakdown and pericentral resynthesis of Gln. CPS functions as a low-affinity but high-capacity system for ammonia detoxification. In the pericentral compartment, ammonia escaping the periportal compartment is used for Gln synthesis (a high-affinity but low-capacity system). Adapted with permission from *European Journal of Biochemistry*[2] and *Frontiers in Bioscience*.[9] (B) Metabolic reactions and compartment volumes considered in the MM. Gln, ammonia (NH_4^+), and urea enter the MM ($c_{Gln,in}$, $c_{NH4,in}$, and $c_{Urea,in}$). Metabolites can be taken up or released by both the periportal and pericentral compartments as indicated by arrows. The volumes of the periportal and pericentral compartments are defined as V_{pp} and V_{pc}, respectively. NH_4^+,endo represents endogenous ammonia sources not considered in detail here. C-bm-P, carbamoyl phosphate.

and necrotic compartments after CCl_4 intoxication and during regeneration.

3. The MM and the STM were coupled to form an integrated metabolic spatial-temporal model (IM), which allowed the prediction of ammonia detoxification in damaged and regenerating livers.
4. For validation, the simulation results of the IM were compared to *in vivo* data for rats and mice. This resulted in good agreement between experimental and simulated data.
5. The investigation was completed with a simplified model of blood circulation with three ammonia-detoxifying compartments in order to estimate the contributions of the (damaged) liver and extrahepatic tissues to ammonia metabolism *in vivo*.

Materials and Methods

Bidirectional Liver Perfusion and Biochemical Assays

All experiments were approved by the responsible local authorities. Male C57BL/6N mice (8-12 weeks old, body weight = 20-25 g, n = 43) were allowed the Ssniff R/M-H diet (Ssniff, Soest, Germany) and water *ad libitum*. Isolated livers were perfused (69 perfusions) without recirculation of the perfusate[17,18] (see also the Supporting Information). In some experiments, a single dose of CCl_4 (1.6 g/kg of body weight) was administered intraperitoneally in corn oil.

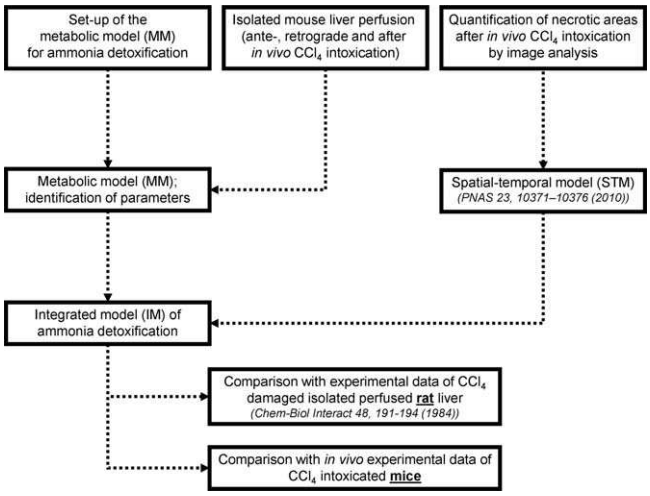

Fig. 2. Work flow for setting up the experiments and models. First, the MM was established on the basis of biological knowledge. Parameters of the model were identified with data from perfusion experiments with isolated livers from healthy and *in vivo* CCl_4-intoxicated mice. With image analysis, the necrotic zones following CCl_4-induced damage and during subsequent liver regeneration were quantified in order to apply the STM.[15] The volume and architectural information allowed the generation of data for the necrotic zone for all time points during damage and regeneration. Combining both models led to the IM for ammonia detoxification of the intact, damaged, and regenerating liver. Finally, the model was validated with published data for ammonia detoxification in isolated, perfused rat livers[5] and with *in vivo* measured liver metabolite concentrations of mice.

Quantification of Metabolites in Mouse Blood for Model Validation

Ammonia, urea, and Gln were measured in plasma obtained from portal and hepatic veins of mice 0 to 12 days after CCl_4 administration. Three mice were used per time point. Ammonia and urea were quantified with kits from Sigma-Aldrich (Taufkirchen, Germany) and BioAssay Systems (Hayward, CA), respectively. Gln was measured with high-performance liquid chromatography at Laborärztliche Arbeitsgemeinschaft für Diagnostik und Rationalisierung Medizinisches Versorgungszentrum (Dortmund, Germany). At each time point, the liver was fixed in 4% paraformaldehyde (Carl-Roth, Karlsruhe, Germany) for 48 hours, and it was used for hematoxylin/eosin staining.

Quantification of Liver Compartment Volumes

The MM uses the volumes of the periportal and pericentral regions (V_{pp} and V_{pc}, respectively) in the lobule in which the ammonia-catabolizing reactions take place. These volumes were estimated with the following relations: $V \approx Nv_H h/L$, $V_{pp} \approx N_{pp}v_H h/L$, and $V_{pc} \approx N_{pc}v_H h/L$. Here, v_H is the hepatocyte volume ($v_H \approx 1.26 \times 10^{-5}$ mm^3), h is the approximate average height of a lobule ($h \approx 279.6$ μm), and L is the average hepatocyte diameter ($L \approx 23.3$ μm).[15] N is the number of hepatocytes within a liver lobule (determined from confocal laser scanning micrographs).[15] N_{pp} and N_{pc} are the periportal and pericentral numbers of hepatocytes in a cross-section of a liver lobule, respectively. They were determined from GS-stained bright-field micrographs. In the intact liver, $N = N_{pp} + N_{pc}$ held. We found $V_{pp} \approx 12V/13$ and $N_{pc} \approx V/13$. The compartment volumes of healthy livers and livers during regeneration were taken from Hoehme et al.[15]

Calculation of the Perfusion Volume Flow

The perfusion volume flow rate per liver mass, $F_{mL} = F/m_L$ (where F is the transported volume per unit of time), was experimentally determined and was, on average, 6 mL·min^{-1}·g^{-1}. It could be used to calculate the term F/V_x for the MM, that is, the ratio of

Table 1. Summary of 69 Mouse Liver Perfusion Experiments

Experiment	Perfusion Direction	$c_{Gln,in}$ (mM)	$c_{NH4,in}$ (mM)	CCl_4	$c_{Gln,out}$ (mM)	SD for $c_{Gln,out}$	$c_{NH4,out}$ (mM)	SD for $c_{NH4,out}$	$c_{Urea,out}$ (mM)	SD for $c_{Urea,out}$
1	Antegrade	0	0	No	0.0169	0.0145	0.0026	0.0045	0.0175	0.0051
2	Antegrade	0	0.2	No	0.0500	0.0174	0.0384	0.0121	0.0467	0.0102
3	Retrograde	0	0	No	0.0040	0.0155	0.0300	0.0115	0.0174	0.0073
4	Retrograde	0	0.2	No	0.0557	0.0141	0.0699	0.0092	0.0328	0.0090
5	Antegrade	0.125	0	No	0.1196	0.0210	0.0063	0.0042	0.0286	0.0037
6	Antegrade	0.25	0	No	0.2387	0.0251	0.0108	0.0055	0.0256	0.003
7	Antegrade	0.5	0	No	0.4912	0.0965	0.0165	0.0055	0.0277	0.0027
8	Antegrade	0.125	0.2	No	0.1867	0.0394	0.0391	0.0101	0.0599	0.0208
9	Antegrade	0.25	0.2	No	0.3089	0.0656	0.0436	0.0084	0.0592	0.0191
10	Antegrade	0.5	0.2	No	0.4848	0.0526	0.0568	0.0083	0.1240	0.0415
11	Antegrade	0	0.2	Yes	0.0000	0.0026	0.1010	0.0407	0.0494	0.0188
12	Antegrade	0.125	0.2	Yes	0.1156	0.0373	0.1075	0.0401	0.0512	0.0234
13	Antegrade	0.125	0	Yes	0.1256	0.0456	0.0269	0.0056	0.0182	0.0102

The table shows the perfusion direction (either antegrade or retrograde), the mean steady-state inflow concentrations of Gln ($c_{Gln,in}$) and ammonia ($c_{NH4,in}$) in the perfusion medium, and the measured mean steady-state outflow concentrations of Gln ($c_{Gln,out}$), ammonia ($c_{NH4,out}$), and urea ($c_{Urea,out}$) with the standard deviations (SDs).

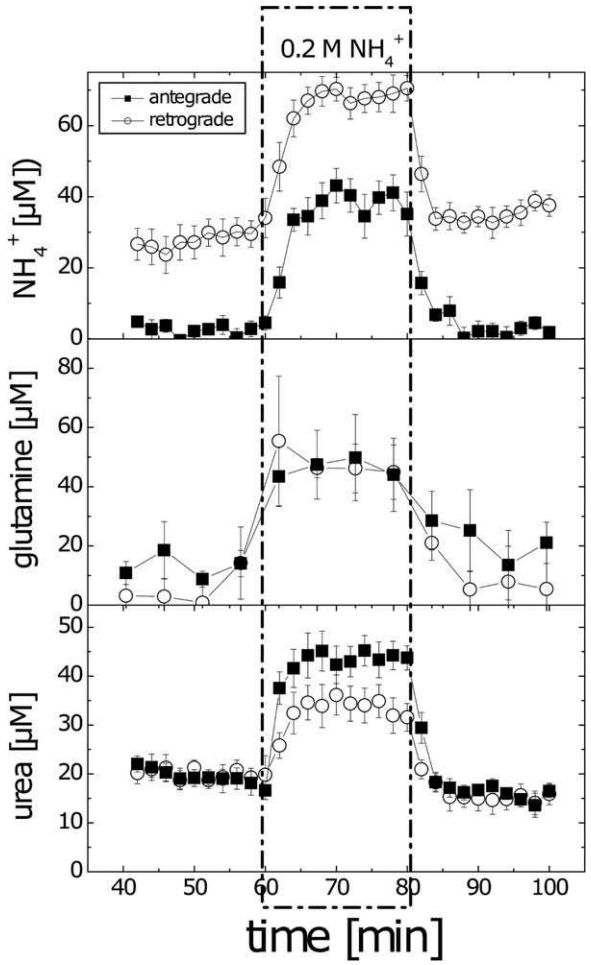

Fig. 3. Impact of the perfusion direction on the involvement of ammonia-detoxifying pathways. Intact, isolated mouse livers were perfused in either the antegrade or retrograde direction throughout the entire perfusion experiment. After 60 minutes of perfusion, 0.2 mM ammonia was added for another 20 minutes to the perfusate. This resulted in an increase in the urea and Gln output. Steady-state conditions were reached within minutes, and these steady-state concentrations were used to fit the parameters of the MM.

flow F and the volume of compartment x [V_x; $x = \mathrm{pp}$ (periportal) or pc (pericentral)]. See also Supporting Equations 1 to 5.

Endogenous Ammonia From Balancing Measured Concentrations

The production rate of released endogenous ammonia ($v_{\mathrm{NH4,endo}}$) was assumed to be equally distributed over all cells along the acinus. It could be calculated from the nitrogen balance of the perfusion experiment concentrations (Table 1). The residual concentrations of endogenous ammonia ($\Delta c_{\mathrm{NH4,endo}}$) resulted in mean values of 0.0395 mM for perfusion experiments without added ammonia and −0.0495 mM for experiments with ammonia. $v_{\mathrm{NH4,endo}}$ was calculated as follows:

$$v_{\mathrm{NH4,endo}} = F_{mL} \cdot \frac{m_L}{V} \cdot \Delta c_{\mathrm{NH4,endo}} = 6 \frac{\mathrm{ml}}{\mathrm{min} \cdot \mathrm{g}} \cdot 1 \frac{\mathrm{g}}{\mathrm{ml}} \cdot \Delta c_{\mathrm{NH4,endo}} \quad (1)$$

This resulted in $v_{\mathrm{NH4,endo}} = 0.237$ mM/min for all experiments without added ammonia and $v_{\mathrm{NH4,endo}} = -0.297$ mM/min for experiments with ammonia, respectively.

Kinetic Parameters Derived From Fitting the Model Outputs to the Measured Data (Nonlinear Optimization)

The remaining kinetic parameters were determined with model fitting, that is, with the least squares (q) between the measured output concentrations ($c_{j,k}$) and the simulated parameter-dependent output concentrations ($\hat{c}_{j,k}$) for $j = \{\mathrm{Gln}, \mathrm{NH_4}, \mathrm{urea}\}$ and $k = 1, \ldots, 13$ experiments weighted by the square of the respective mean concentrations over all experiments ($\bar{c}_j = \sum_{k=1}^{13} c_{j,k}/13$):

$$q = \sum_{k=1}^{13} \frac{\left(c_{\mathrm{Gln,k}} - \hat{c}_{\mathrm{Gln,k}}\right)^2}{\bar{c}^2_{\mathrm{Gln}}} + \sum_{k=1}^{13} \frac{\left(c_{\mathrm{NH4,k}} - \hat{c}_{\mathrm{NH4,k}}\right)^2}{\bar{c}^2_{\mathrm{NH4}}} + \sum_{k=1}^{13} \frac{\left(c_{\mathrm{Urea,k}} - \hat{c}_{\mathrm{Urea,k}}\right)^2}{\bar{c}^2_{\mathrm{Urea}}} \stackrel{!}{=} \min. \quad (2)$$

Results

Ammonia Detoxification in the Murine Liver: Bidirectional Liver Perfusion Experiments Illustrate the Acinar Zonation of Ammonia Detoxification

During antegrade perfusion and in the absence of exogenous ammonia, only minor amounts of urea and Gln were released (Fig. 3). Upon an infusion with 0.2 mM ammonia (60 minutes after the start of the experiment), a rapid increase in the release of urea and Gln and a surplus of ammonia were detected, and this achieved effluent steady-state conditions within

Table 2. Modeled Reactions

	Main Enzyme	Compartment	Reaction
v_G	GLNase	Periportal	$\mathrm{Gln} \rightarrow \mathrm{NH_4^+} + \mathrm{Glu}$
v_C	CPS	Periportal	$\mathrm{NH_4^+} + \mathrm{HCO_3^-} + \mathrm{Asp} \rightarrow \mathrm{urea} + \mathrm{fumarate}$
v_{GS}	GS	Pericentral	$\mathrm{NH_4^+} + \mathrm{Glu} \rightarrow \mathrm{Gln}$

The symbol, rate limiting enzyme, compartment and overall chemical equation are shown for each of the modeled reactions.

minutes. After the removal of exogenous ammonia, the system returned to the starting conditions.

In contrast to antegrade perfusion, small amounts of ammonia were released from the liver during retrograde perfusion (Fig. 3). This can be explained by a net hepatocellular production of ammonia downstream of the GS-containing pericentral scavenger cells.[19]

Accordingly, antegrade ammonia infusion resulted in lower effluent ammonia concentrations in comparison with retrograde infusion (Fig. 3). Similar results were obtained with an intra-experimental change in the perfusion direction (Supporting Fig. 3). Therefore, it can be hypothesized that the two-compartment model of ammonia detoxification, previously established for rats,[2] may also apply to the intact mouse liver.

In antegrade perfusion experiments using intact livers and livers from *in vivo* CCl_4-intoxicated mice, the input concentrations of Gln and ammonia in the perfusion buffer were changed to various combinations. A functional impairment of 100% for the pericentral compartment and a functional impairment of 15% for the periportal compartment were determined experimentally in mouse livers 4 days after CCl_4 intoxication. This set of 13 mouse liver perfusion conditions formed the basis of the MM (Table 1).

Establishment of the MM

Model Equations. Hepatic ammonia detoxification is confined to the periportal and pericentral compartments (Fig. 1A). Consequently, the MM considers one periportal compartment and one pericentral compartment (Fig. 1B). It integrates over the transport of metabolites into and out of each compartment as well as the main biochemical pathways/reactions within each compartment (for a summary, see Table 2).

Equation 3 describes GLNase-catalyzed Gln degradation (v_G), which includes Hill-type kinetics for Gln and product activation by ammonia[2,20,21]:

$$v_G = v_{max,G} \cdot \frac{c_{Gln,pp}^n}{K_{A,G,Gln}^n + c_{Gln,pp}^n} \cdot \frac{c_{NH4,pp}}{K_{m,G,NH4} + c_{NH4,pp}} \quad (3)$$

where $c_{Gln,pp}$ is the concentration of Gln in the periportal compartment and $c_{NH4,pp}$ is the concentration of NH_4^+ in the periportal compartment. This rate equation is parameterized by the maximal velocity of Gln degradation ($v_{max,G}$), the dissociation constant of Gln ($K_{A,G,Gln}$), the Michaelis constant of ammonia ($K_{m,G,NH4}$), and the Hill coefficient (n). Urea synthesis via the urea cycle consists of five reactions that convert two amino groups, one from NH_4^+ and one from aspartate (Asp), into the excretion product urea. In this work, it is simplified and represented by one of the rate-limiting reactions: carbamoyl phosphate synthetase (CPS). Therefore, the synthesis of urea (v_C) is described as follows:

$$v_C = v_{max,C} \cdot \frac{c_{NH4,pp}}{K_{m,C,NH4} + c_{NH4,pp}} \quad (4)$$

where $v_{max,C}$ represents the maximal synthesis rate of urea and $K_{m,C,NH4}$ is the Michaelis constant of CPS.

Correspondingly, Equation 5 represents the reaction kinetics of Gln synthesis (v_{GS}), which includes activation by ammonia and noncompetitive inhibition by Gln[22]:

$$v_{GS} = v_{max,GS} \cdot \frac{c_{NH4,pc}}{K_{m,GS,NH4} + c_{NH4,pc}} \cdot \frac{K_{i,GS,Gln}}{K_{i,GS,Gln} + c_{Gln,pc}} \quad (5)$$

where $v_{max,GS}$ is the maximal rate of Gln synthesis, $K_{m,GS,NH4}$ is the Michaelis constant of GS, $K_{i,GS,Gln}$ is the inhibition constant, $c_{Gln,pc}$ is the concentration of Gln in the pericentral compartment, and $c_{NH4,pc}$ is the concentration of NH_4^+ in the pericentral compartment. On the basis of these rate equations, $c_{Gln,pp}$, $c_{NH4,pp}$, and the concentration of urea of the periportal compartment ($c_{Urea,pp}$) can be described by 3 differential equations that reflect the mass balance:

$$V_{pp} \frac{dc_{Gln,pp}}{dt} = -v_G V_{pp} + (c_{Gln,in} - c_{Gln,pp}) F \quad (6)$$

$$V_{pp} \frac{dc_{NH4,pp}}{dt} = (v_G - v_C) V_{pp} + (c_{NH4,in} - c_{NH4,pp}) F + v_{NH4,endo} V_{pp} \quad (7)$$

$$V_{pp} \frac{dc_{Urea,pp}}{dt} = v_C V_{pp} + (c_{Urea,in} - c_{Urea,pp}) F \quad (8)$$

where V_{pp} is the volume of the periportal compartment in the intact liver ($V_{pp} \approx 12 V_{pc}$), $c_{Gln,in}$ is the inflow concentration of Gln, $c_{NH4,in}$ is the inflow concentration of NH_4^+, and $c_{Urea,in}$ is the inflow concentration of urea. During regeneration, the volume changes with time: $V = V(t)$, $V_{pp} = V_{pp}(t)$, and $V_{pc} = V_{pc}(t)$. The volume changes occur much more slowly than the changes in the metabolite concentrations. Hence, the volume can be considered to be quasi-stationary during changes in the metabolite concentration. F denotes the volumetric perfusion flow rate (i.e., the transported volume per unit of time). Because transport processes are assumed to occur instantaneously in this model, F drives the transport of input metabolites (e.g., incoming blood with $c_{Gln,in}$) and periportal output metabolites (e.g., $c_{Gln,pp}$). For ammonia (Equation 7), there is an additional term representing the endogenous

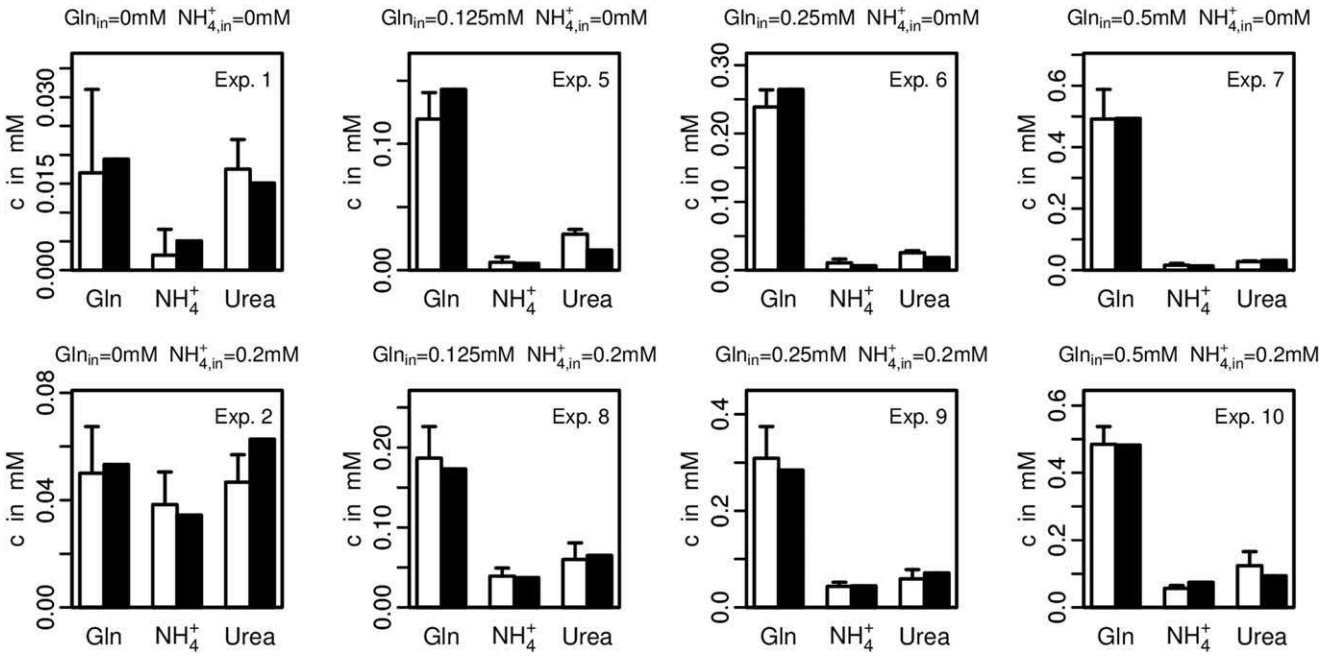

Fig. 4. Measured and simulated steady-state outflow concentrations of Gln, ammonia, and urea show good agreement between the MM predictions and the experimental data from intact mouse liver perfusions in the antegrade direction. The white bars show the measured outflow concentrations and the standard deviations. The black bars represent the simulation results. The inflow concentrations of Gln (Gln_{in}) and ammonia ($NH_4^+{}_{in}$) in the perfusion medium are given at the top of each plot. Numbers in the boxes refer to the experiments listed in Table 1.

ammonium production rate: $v_{NH4,endo}$ (see Equation 1). It is located inside the compartment (Fig. 1B) and represents further ammonia fluxes such as intercellular protein degradation[19] and nonmodeled reactions. Similarly, there are 3 differential equations for the pericentral compartment:

$$V_{pc}\frac{dc_{Gln,pc}}{dt} = v_{GS}\,V_{pc} + (c_{Gln,pp} - c_{Gln,pc})F \quad (9)$$

$$V_{pc}\frac{dc_{NH4,pc}}{dt} = -v_{GS}\,V_{pc} + (c_{NH4,pp} - c_{NH4,pc})F + v_{NH4,end}\,V_{pc} \quad (10)$$

$$V_{pc}\frac{dc_{Urea,pc}}{dt} = (c_{Urea,pp} - c_{Urea,pc})F \quad (11)$$

where $c_{Urea,pc}$ is the concentration of urea in the pericentral compartment. In addition, the model allows us to simulate retrograde perfusion with the following substitutions (Fig. 1B): (1) $c_{Gln,pp}$, $c_{NH4,pp}$, and $c_{Urea,pp}$ in Equations 9-11 become $c_{Gln,in}$, $c_{NH4,in}$, and $c_{Urea,in}$, respectively, and (2) $c_{Gln,in}$, $c_{NH4,in}$, and $c_{Urea,in}$ in Equations 6-8 become $c_{Gln,pc}$, $c_{NH4,pc}$, and $c_{Urea,pc}$, respectively.

Theoretically, in impaired liver tissue, a third compartment comprising the necrotic tissue could be added. This compartment is metabolically not active and, for reasons of simplicity, was neglected for the calculation of metabolites (Supporting Equations 6-8).

Determination of the Parameter Values. The volumes and the flow parameters as well as the endogenous ammonia rates were calculated from measured data (Equation 1 and Table 1). The Hill coefficient of GLNase (n) was set to the reported value of 2.[21] The remaining kinetic parameters were determined by the least squares (q; Equation 2) between the measured (Table 1) and simulated steady-state concentrations of Gln, ammonia, and urea. Supporting Table 1 shows the resulting fitted parameter. It is noticeable that the $K_{m,C,NH4}$ value of the CPS reaction is more than 100-fold higher than the $K_{m,GS,NH4}$ value of the GS reaction; this reflects the high-capacity/low-affinity and low-capacity/high-affinity compartments originally described by Häussinger.[2]

Model Simulations of Experimental Perfusion Data. With the fitted parameters derived from the perfusion experiments, the Gln, ammonia, and urea concentrations were calculated with the MM. The simulated and experimentally determined concentrations were in good quantitative and qualitative agreement (Fig. 4). Besides simulation of antegrade perfusion, the model also allows simulation of retrograde perfusion (Supporting Fig. 4) as well as perfusion experiments with CCl_4-intoxicated livers (Supporting Fig. 5).

A strength of the MM is its ability to calculate not only the output concentrations of NH_4^+, Gln, and urea at any given input concentration but also the concentrations of the metabolites at the border between the periportal and pericentral compartments (Supporting Table 2).

In summary, despite its simplicity, the MM with two compartments is capable of explaining the experimental findings of hepatic ammonia detoxification.

Development of an IM

Compartment modeling, as described in the previous paragraph, does not consider the complex spatial-temporal changes in cellular tissue architecture after liver damage and during regeneration. In particular, it does not explain volume changes in the subcompartments occurring after CCl_4-induced damage. In order to circumvent these limitations, an integrated mathematical model (IM), based on the STM[15] in combination with the previously described MM, was developed.

Briefly, the STM model is a center-based (single cell–based) model[23] based on the following model assumptions (for details, see Hoehme et al.[15]):

1. Hepatocytes can be mimicked as homogeneous, isotropic, elastic and adhesive, intrinsically spherical objects capable of migration, growth, division, and death.
2. The migration of each hepatocyte can be calculated with an equation of motion. This equation permits us to investigate the position and orientation of each hepatocyte at each instant of time by summing up all physical forces, including active force components such as micromotility. The physical forces include friction forces of hepatocytes with the extracellular matrix, the sinusoids, and other hepatocytes as well as repulsion and adhesion forces of a hepatocyte within its environment.
3. Cell orientation changes can be mimicked by an optimization principle with the Metropolis algorithm for the energy change occurring in case of a cell orientation change.[24] Alternatively, an equation for the angular momentum[25] can be used, but such an equation is much more complicated and computationally more expensive.
4. The hepatocytes have been assumed to divide along the closest sinusoid. This order principle ensures the regeneration of liver architecture.[15]
5. The model considers only sinusoids and hepatocytes, the main constituents of a liver lobule. Other cell types are neglected. The sinusoidal network is mimicked through chains of spheres linked by springs, and each sphere is again modeled by an equation of motion. In this way, the interaction forces between hepatocytes and sinusoids can be efficiently modeled.

The STM quantitatively mimics the regeneration of the liver mass and architecture after CCl_4-induced pericentral damage.[15] The volumes of the periportal and pericentral compartments were calculated with the STM and were subsequently inserted into the MM. Thus, the two models were coupled.

Moreover, in order to visualize the metabolism calculated with the MM and the STM in time and space, the concentrations of Gln, ammonia, and urea at any given point in time and space were approximated with a mathematical interpolation approach. The MM provided the concentrations of ammonia, urea, and Gln at (A) the central vein, (B) an intermediate region at the border between the GS-positive and GS-negative parts of the lobule, and (C) the portal triads during the entire regeneration process after CCl_4 intoxication. With these data, we performed a two-stage, *n*-linear interpolation in space, which is a direct extension of bilinear interpolation, within a two-dimensional hexagonal polygon aligned orthogonally to the central vein in order to interpolate the concentration values at any point in space (see Equations 12 and 13) and time (see Equation 14) within a liver lobule:

$$C_{AB}(t) = C_A(t) + (C_B(t) - C_A(t)) \frac{x_A}{(x_A + x_B)} \quad (12)$$

$$C_{BC}(t) = C_B(t) + (C_C(t) - C_B(t)) \frac{x_B}{(x_B + x_C)} \quad (13)$$

$$C_{AC}(t_{i,i+1}) = C_{AC}(t_i) + (C_{AC}(t_{i+1}) - C_{AC}(t_i)) \frac{t_{i,i+1} - t_i}{t_{i+1} - t_i} \quad (14)$$

where $C_A(t)$, $C_B(t)$, and $C_C(t)$ are the concentrations at positions *A*, *B*, and *C*, respectively. $C_{AB}(t)$ is the concentration at a given point in space between *A* and *B*. $C_{BC}(t)$ and $C_{AC}(t)$ are defined accordingly. In Equations 12 and 13, which represent the spatial interpolation, x_A is the minimal distance of that point to *A*, and x_B and x_C are defined accordingly. In equation 14, which represents the temporal interpolation, $t_{i,i+1}$ is a given point in time between t_i and t_{i+1}.

The IM simulates the concentrations of ammonia, urea, and Gln in the liver vein after CCl_4-induced tissue destruction and the regeneration process. Figure 5A summarizes the destruction and regeneration of the two compartments and the corresponding changes in the metabolites. For this simulated liver perfusion

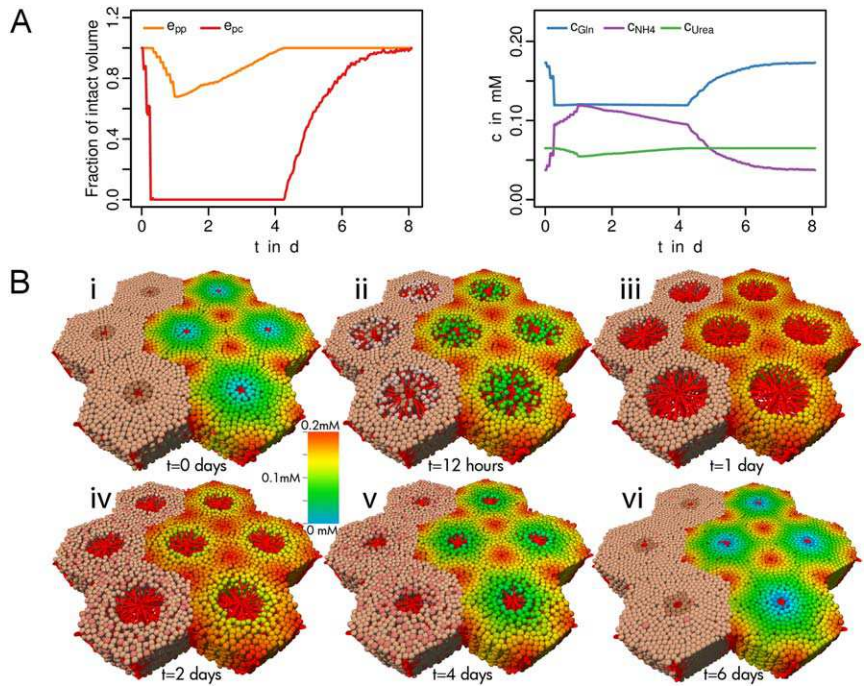

Fig. 5. (A) Simulation of the acinar compartment volumes and metabolite concentrations over time during the damage and regeneration of livers from CCl_4-intoxicated mice. The time courses of the periportal fractions ($e_{pp} \propto V_{pp}$) and pericentral fractions ($e_{pc} \propto V_{pc}$) of the intact volume after *in vivo* CCl_4 intoxication of mice (top left) with the corresponding changes in c_{Gln}, c_{NH4}, and c_{Urea} (top right) are shown. Metabolite concentrations were calculated via the MM with the impaired volumes as quantified by the STM. (B) Simulated damage and regeneration scenario with the IM. The individual figures show seven neighboring liver lobules over time under intact, damaged, and regenerating conditions. Vessels are denoted by red elements. The left three lobules show normal hepatocytes (light brown), GS-positive hepatocytes (dark brown), proliferating hepatocytes (red, pink-like color), and the necrotic zone (empty pericentral space). The right four lobules show the local ammonia concentration according to the color legend. The visualization of the ammonia concentration was calculated with an interpolation algorithm using the metabolic compartment model: (i) intact liver lobules, (ii) necrosis in progress after CCl_4 intoxication, (iii) maximum necrosis, (iv) onset of regeneration, (v) beginning of the regeneration of the pericentral compartment, and (vi) final stages of regeneration. A video sequence of this process and the corresponding concentrations of ammonia, Gln, and urea is provided as Supporting Information.

during regeneration, the input concentrations were kept constant at $c_{Gln,in} = 0.125$ mM and $c_{NH4,in} = 0.2$ mM (Fig. 5A), and a flow rate of 6 $mL \cdot min^{-1} \cdot g^{-1}$ was applied.

Notice that the previously established model comprising only one liver lobule[15] was extended in Fig. 5B to a group of seven lobules. The seven-lobule configuration reduced boundary artifacts that emerged if only a single lobule was considered (data not shown). Each lobule was created on the basis of statistical data obtained from an analysis of 26 confocal volume data sets. Therefore, Fig. 5B represents statistical lobules with average properties. This novel IM allowed us to (1) calculate the development of the total volume of hepatocytes in the periportal and pericentral compartments at any time during the tissue destruction and regeneration process and (2) calculate and visualize the concentrations of ammonia, urea, and Gln for each individual cell (see the video in the Supporting Information).

Comparison of the Model Predictions to Experimental Data and Implications. Results simulated by the IM were validated with experimental data from both rats and mice. First, data published by Häussinger and Gerok[5] showed that the perfusion of isolated intact rat livers with increasing ammonia concentrations resulted in increasing ammonia release, an increase in released Gln, and a linear increase in urea (Fig. 6A-C). In isolated, perfused livers from CCl_4-intoxicated rats, the concentration of released ammonia was higher than that in livers from control animals. Almost no Gln synthesis occurred because of the destroyed pericentral compartment, whereas urea synthesis remained largely unaffected. Even though the model parameters were calibrated with perfusion data from isolated mouse livers, the MM was able to correctly simulate the metabolic changes after CCl_4 administration (Fig. 6D-F). Furthermore, this indicates that the underlying mechanisms governing ammonia detoxification are highly comparable in mice and rats.

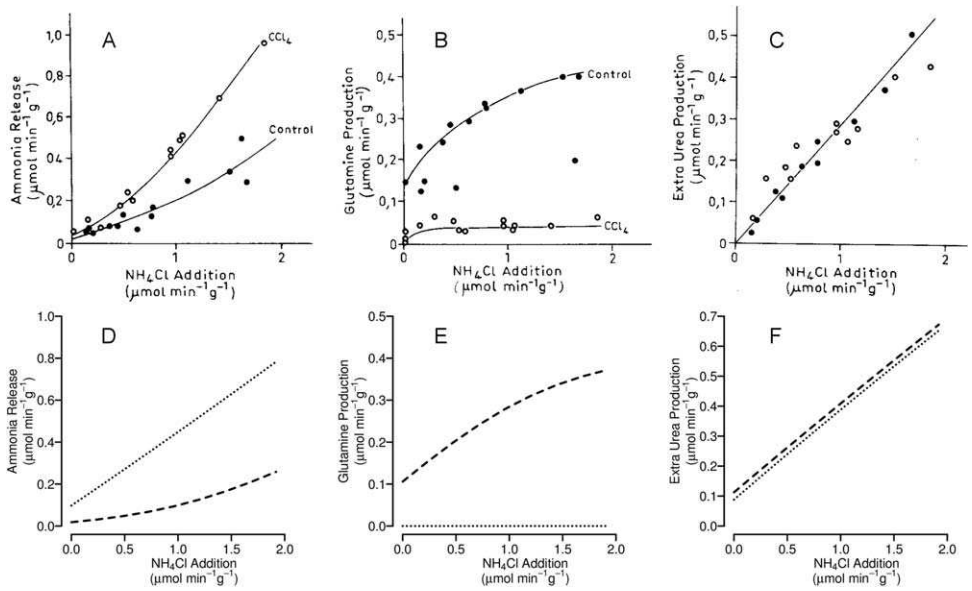

Fig. 6. Model results versus published data for perfusion experiments using isolated livers from CCl_4-intoxicated rats. In the top row, published data show that CCl_4 intoxication of rat livers results in (A) increased ammonia release, (B) a strong decrease in Gln synthesis, and (C) essentially no effects on urea synthesis. Reprinted with permission from *Chemico-Biological Interactions*.[5] Copyright 1984, Elsevier. The bottom row presents a simulation of these experiments with the MM. A comparison of the top row and the bottom row shows good qualitative agreement despite calibration of the model based on data from mouse livers. This demonstrates the general validity of the model at least for the rodent liver.

Second, mice were intoxicated *in vivo* with CCl_4 to induce severe liver damage. Blood was taken from the portal vein (representing the liver inflow) and the liver vein (representing the liver outflow) at different time points after CCl_4 intoxication (Fig. 7). Assuming that the ratio of arterial blood to venous blood at the portal site was 3:7[26] and that the concentrations of ammonia and Gln in the right heart chamber were similar to those in the hepatic artery, we were able to calculate the input concentrations of the liver on the basis of the concentrations determined *in vivo* for the right heart chamber (Supporting Fig. 6) and the portal vein. These concentrations were used as input parameters (meas,in, measured liver input values). For the simulations with the MM, the profiles depicted in Fig. 5A were used at a physiological flow rate of 4 $mL \cdot min^{-1} \cdot g^{-1}$.[27] The concentrations in the hepatic vein were predicted for two different rates of endogenous ammonia and were compared with experimental *in vivo* data (Fig. 7). Although the predicted and experimentally determined concentrations of ammonia and Gln almost perfectly matched in the normal and fully regenerated mice and nicely followed the strong changes after damage and during regeneration, the quantitative fit during this period was slightly less. This may indicate so far unknown aspects of ammonia detoxification in damaged livers.

It is well known that extrahepatic organs such as the skeletal muscles, brain, and kidneys may contribute to ammonia metabolism.[28] To understand the influence of these extrahepatic compartments, we used the previously described mouse hepatotoxicity protocol with CCl_4. Ammonia and Gln were analyzed in the portal and liver veins and additionally in mixed venous blood from the right heart chamber (Supporting Fig. 6). With the data, the extrahepatic contribution was calculated on the basis of a three-compartment model (Supporting Fig. 7) consisting of (1) the liver, (2) organs in series with the liver (e.g., the gastrointestinal tract, including the gut and splanchnic organs; extrahepatic 2), and (3) extrahepatic organs parallel to the liver (e.g., skeletal muscles, kidneys, and brain; extrahepatic 1). The model showed that the extrahepatic 1 compartment switched from a neutral state to extrahepatic ammonia detoxification during days 2 to 4 after CCl_4 administration with a maximal rate of 0.24 μmol/min (Supporting Fig. 8). Correspondingly, extrahepatic Gln formation increased during the same period. In contrast, the compartment of the gastrointestinal tract (extrahepatic 2) did not show any significant changes after CCl_4 intoxication.

Analyzing the concentrations of 13 amino acids in the portal and hepatic liver veins and the right heart chamber, we observed a rather complex situation. For example, 2 days after CCl_4 intoxication, the serum concentration of aspartic acid increased, and liver aspartic acid metabolism seemed to be impaired. In contrast, only minor changes in histidine were observed, whereas

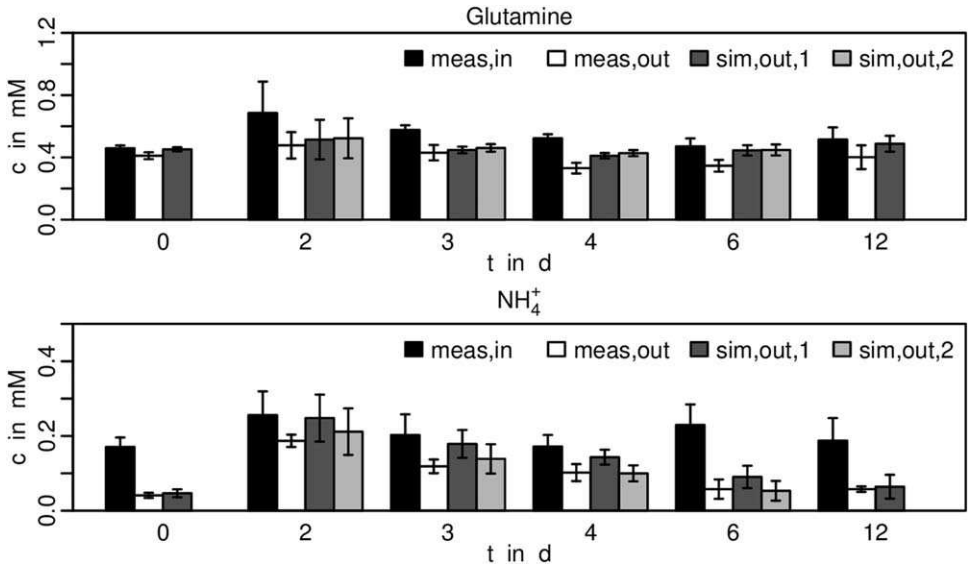

Fig. 7. *In vivo* model validation using *in vivo* ammonia and Gln concentrations during liver regeneration after CCl_4 intoxication of mice. Experimentally determined liver input concentrations (meas,in), composed of arterial and portal blood in a 3:7 ratio[26] of Gln (top) and ammonia (bottom) were used to predict the respective output concentrations in the hepatic vein (sim,out,1) and were compared with the experimentally measured concentrations (meas,out). For these experiments, no endogenous ammonia source was considered, i.e. $v_{NH4,endo} = 0$ mM/min. On days 0 and 12, a very good quantitative prediction can be made, particularly for ammonia. In necrotic tissue and during regeneration (days 2-6), the predicted values (sim,out,1) closely mimic the observed changes. However, the simulated concentrations of ammonia are slightly higher than those determined experimentally. Taking into account an ammonia sink by setting $v_{NH4,endo}$ to -0.297 mM/min improves the simulation (sim,out,2) for the regeneration phase (days 2-6), and this indicates that additional, yet unidentified mechanisms of ammonia removal might play a role during regeneration. Meas,in, measured liver input values; meas,out, measure liver output values; sim,out,1, simulated liver output values for $v_{NH4,endo} = 0$ mM/min; sim,out,2, simulated liver output values for $v_{NH4,endo} = -0.297$ mM/min.

arginine (Arg) disappeared completely from the circulation (Supporting Figs. 9 and 10).

Discussion

In this study, an MM of hepatic ammonia metabolism was developed and combined with an STM[15] into an IM simulating the impact of liver damage and regeneration after intoxication on ammonia detoxification. The MM represents the main reactions of ammonia detoxification and their zonal distribution in liver lobules. Numerical model fitting resulted in excellent agreement between the model outputs and the experimental data from antegrade and retrograde isolated, perfused mouse livers. The IM allows us for the first time to simulate and visualize whether, where, and to what extent liver damage compromises ammonia detoxification. Although established for CCl_4, the model can be easily adapted to other hepatotoxins known to induce zonal liver damage. Thus, the user can choose a certain extent and spatial pattern of liver damage in order to calculate the concentrations of ammonia, Gln, and urea in the hepatic vein (liver outflow) for given concentrations of the three metabolites in the portal vein (liver inflow).

The model calculations were compared with corresponding data from two experimental scenarios. The first scenario (Fig. 6) was related to data from isolated, perfused livers of rats with and without pretreatment with hepatotoxic doses of CCl_4.[5] The model simulations were in good agreement with the experimental data. This is remarkable because the model established here was calibrated with mouse livers and demonstrated its general validity at least for rodent livers.

The second experimental scenario was related to data from CCl_4-intoxicated mice *in vivo* over a period of 12 days (Fig. 7). The concentrations of ammonia, Gln, and urea were analyzed in the portal and hepatic veins of the mice at different time periods after intoxication. Assuming that the compartment volume changes during damage and regeneration were much slower than the concentration changes *in vivo*, we found that the data simulated by the IM closely followed the experimentally observed changes in the outflow concentrations during tissue damage and regeneration, although the match was not as perfect as that for a normal liver.

Differences between simulated and experimental data offer us the opportunity to identify still unknown physiological mechanisms. The model allows the testing of hypothetical reactions and whether they improve simulation accuracy. If an additional (yet unknown) sink of ammonia in damaged and regenerating livers is simulated by the setting of $v_{NH4,endo}$ to -0.297 mM/min,

the agreement between experimental and simulated data considerably improves (Fig. 7). A possible ammonia sink might be the *de novo* synthesis of amino acids (and proteins). An increase in the latter during liver regeneration is well known.

Furthermore, the incorporation of the IM into a simplified model of blood circulation with three ammonia-detoxifying compartments allowed the estimation of the relative contributions of the (damaged) liver and extrahepatic tissues to amino acid and ammonia metabolism *in vivo*. Interestingly, this resulted in a demonstration of increased extrahepatic ammonia detoxification and the discovery of an altered amino acid metabolism [e.g., Arg (cf. Supporting Fig. 9) or Asp (cf. Supporting Fig. 10)] during regeneration after CCl_4.

These examples illustrate how the model may help us to distinguish realistic hypotheses from unrealistic ones and to better interpret changes in altered serum amino acid levels in diseased states.

In conclusion, an MM of ammonia detoxification was successfully merged with an STM of tissue damage and regeneration. The resulting integrated model nicely predicted ammonia detoxification in the intact or toxin-damaged and regenerating liver. The integrated liver model is programmed so that it can be easily coupled to models of other body compartments and thus represents a valuable step on the path to virtual organisms.

Acknowledgment: The authors thank N. Eichhorst, F. Struck, and D. Mahn for their excellent technical assistance and S. Töpfer and I. Vignon-Clementel for valuable discussions. The administrative support of G. Miczka and E. Stüttgen at the Projektträger Jülich is also gratefully acknowledged.

References

1. Häussinger D, Schliess F. Pathogenetic mechanisms of hepatic encephalopathy. Gut 2008;57:1156-1165.
2. Häussinger D. Hepatocyte heterogeneity in glutamine and ammonia metabolism and the role of an intercellular glutamine cycle during ureogenesis in perfused rat liver. Eur J Biochem 1983;133:269-275.
3. Gebhardt R, Mecke D. Heterogeneous distribution of glutamine synthetase among rat liver parenchymal cells *in situ* and in primary culture. EMBO J 1983;2:567-570.
4. Görg B, Wettstein M, Metzger S, Schliess F, Häussinger D. Lipopolysaccharide-induced tyrosine nitration and inactivation of hepatic glutamine synthetase in the rat. HEPATOLOGY 2005;41:1065-1073.
5. Häussinger D, Gerok W. Hepatocyte heterogeneity in ammonia metabolism—impairment of glutamine synthesis in CCl_4 induced liver cell necrosis with no effect on urea synthesis. Chem Biol Interact 1984;48:191-194.
6. Häussinger D, Lamers WH, Moorman AFM. Hepatocyte heterogeneity in the metabolism of amino acids and ammonia. Enzyme 1992;46:72-93.
7. Gebhardt R, Baldysiak-Figiel A, Krügel V, Ueberham E, Gaunitz F. Hepatocellular expression of glutamine synthetase: an indicator of morphogen actions as master regulators of zonation in adult liver. Prog Histochem Cytochem 2007;41:201-266.
8. Moorman AFM, de Boer PAJ, Watford M, Dingemanse MA, Lamers WH. Hepatic glutaminase mRNA is confined to part of the urea cycle domain in the adult rodent liver lobule. FEBS Lett 1994;356:76-80.
9. Häussinger D, Schliess F. Glutamine metabolism and signaling in the liver. Front Biosci 2007;12:371-391.
10. Kaiser S, Gerok W, Häussinger D. Ammonia and glutamine metabolism in human liver slices: new aspects on the pathogenesis of hyperammonemia in chronic liver disease. Eur J Clin Invest 1988;18:535-542.
11. Blei AT. The pathophysiology of brain edema in acute liver failure. Neurochem Int 2005;47:71-77.
12. Kuchel PW, Roberts DV, Nichol LW. Simulation of urea cycle: correlation of effects due to inborn errors in catalytic properties of enzymes with clinical-biochemical observations. Immunol Cell Biol 1977;55:309-326.
13. Fellenz W, Häussinger D. Control of acid-base and ammonia homeostasis by the liver. WSEAS Transact Biol Biomed 2004;1:294-297.
14. Hoehme S, Drasdo D. A cell-based simulation software for multicellular systems. Bioinformatics 2010;26:2641-2642.
15. Hoehme S, Brulport M, Bauer A, Bedawy E, Schormann W, Hermes M, et al. Prediction and validation of cell alignment along microvessels as order principle to restore tissue architecture in liver regeneration. Proc Natl Acad Sci U S A 2010;107:10371-10376.
16. Holzhütter HG, Drasdo D, Preusser T, Lippert J, Henney AM. The virtual liver: a multidisciplinary, multilevel challenge for systems biology. Wiley Interdiscip Rev Syst Biol Med 2012;4:221-235.
17. vom Dahl S, Häussinger D. Experimental methods in hepatology. Guidelines of the German Association for the Study of the Liver (GASL). Liver perfusion—technique and applications. Z Gastroenterol 1997;35:221-226.
18. Gohla A, Klement K, Piekorz RP, Pexa K, vom Dahl S, Spicher K, et al. An obligatory requirement for the heterotrimeric G protein Gi3 in the antiautophagic action of insulin in the liver. Proc Natl Acad Sci U S A 2007;104:3003-3008.
19. Schimassek H, Gerok W. Control of the levels of free amino acids in plasma by the liver. Biochem Z 1965;343:407-415.
20. McGivan JD, Bradford NM. Characteristics of the activation of glutaminase by ammonia in sonicated rat liver mitochondria. Biochim Biophys Acta 1983;759:296-302.
21. Patel M, McGivan JD. Partial purification and properties of rat liver glutaminase. Biochem J 1984;220:583-590.
22. Deuel TF, Louie M, Lerner A. Glutamine synthetase from rat liver. Purification, properties, and preparation of specific antisera. J Biol Chem 1978;253:6111-6118.
23. Anderson ARA. A hybrid multiscale model of solid tumor growth and invasion: evolution and the microenvironment. In: Anderson ARA, Chaplain MAJ, Rejniak KA, eds. Single-Cell-Based Models in Biology and Medicine. Basel, Switzerland: Birkhäuser; 2007:3-28.
24. Drasdo D. Center-based single-cell models: an approach to multi-cellular organization based on a conceptual analogy to colloidal particles. In: Anderson ARA, Chaplain MAJ, Rejniak KA, eds. Single-Cell-Based Models in Biology and Medicine. Basel, Switzerland: Birkhäuser; 2007:171-196.
25. Drasdo D, Hoehme S. A single-cell-based model of tumor growth *in vitro*: monolayers and spheroids. Phys Biol 2005;2:133-147.
26. Ekataksin W, Kaneda K. Liver microvascular architecture: an insight into the pathophysiology of portal hypertension. Semin Liver Dis 1999;19:359-382.
27. Cornford EM, Braun LD, Pardridge WM, Oldendorf WH. Blood flow rate and cellular influx of glucose and arginine in mouse liver *in vivo*. Am J Physiol 1980;238:H553-H560.
28. Olde Damink SW, Jalan R, Dejong CH. Interorgan ammonia trafficking in liver disease. Metab Brain Dis 2009;24:169-181.

Supporting Information

Additional Supporting Information may be found at onlinelibrary.wiley.com/doi/10.1002/hep.27136/suppinfo.